Batteries & Supercaps

Research Article
doi.org/10.1002/batt.202400159

Chemistry Europe
European Chemical Societies Publishing

www.batteries-supercaps.org

Agar-Based Interface for Suppressing Parasitic Reactions toward High-Performance Aqueous Zn-Ion Batteries

Yi-Fan Qu,[a] Xin Liu,[a] Jia-Wei Qian,[a] Jingwei Chen,*[b] and Li-Feng Chen*[a]

With advantages including high capacity, intrinsic safety and low cost, aqueous zinc-ion batteries (AZIBs) are ideal electrochemical energy storage devices for large-scale and portable energy storage. However, the development of AZIBs suffers from tricky challenges, such as the notorious Zn dendrite growth and severe parasitic reactions. Herein, as a low-cost and nontoxic biomass, agar is adopted to construct an interface layer on Zn foil to mitigate side reactions and induce uniform Zn deposition on Zn anodes. The interaction between Zn^{2+} and polar functional groups of agar can regulate Zn^{2+} distribution and promote Zn^{2+} desolvation, thus simultaneously achieving homogenous Zn deposition and suppressed hydrogen evolution reaction. Meanwhile, SO_4^{2-} anions are blocked from contacting Zn surface due to electrostatic repulsion, greatly restraining corrosion and passivation. Consequently, Zn||A-Cu asymmetric cell operates normally for 590 cycles with an average coulombic efficiency of 99.5%, suggesting good reversibility of Zn plating/stripping. Notably, A-Zn symmetric cell exhibits a long lifespan of 1100 h at 2 mA cm^{-2}. Furthermore, the A-Zn||NVO full cell displays a superb capacity retention of 94.8% after 3600 cycles at 5 A g^{-1}. This work offers a novel interface modification method for constructing stable and dendrite-free anodes of AZIBs.

Introduction

The issues brought by excessive exploitation and utilization of fossil fuel propel the rapid development of renewable energy.[1] Meanwhile, electrochemical energy storage devices with high energy density have been designed to adjust the temporal and spatial distribution of electric energy produced by renewable resources.[2] Aqueous zinc-ion batteries (AZIBs) become one of the most promising candidates due to their inherent advantages, such as high capacity (820 mAh g^{-1} and 5855 mAh cm^{-3}), low redox potential (−0.762 V vs. standard hydrogen electrode), low price and high safety.[3] Nevertheless, hydrogen evolution reaction (HER), corrosion, passivation and notorious Zn dendrite on Zn anodes pose great threats to the advancement of high-performance AZIBs.[4]

In this case, a number of strategies have been proposed to optimize the electrochemical performance of Zn anodes, such as electrolyte engineering,[5] substrate engineering,[6] separator optimization,[7] and interface modification.[8] Since parasitic reactions and dendrite growth usually take place at the electrode/electrolyte interphase, interface modification is regarded as one of the most effective and direct methods to stabilize Zn anodes.[9] Recently, various kinds of materials have been utilized as interface layers, including inorganic materials (ZnS, Sb_2O_3, TiO_2, hydroxyapatite),[10] carbonaceous materials (CNTs, graphdiyne),[11] alloys (AgZn, InSn, ZnCo),[12] polymers (polyaniline, polydopamine, polyamide),[13] and so on. However, most of these materials are toxic or nondegradable, and their synthesis and preparation are normally complicated and energy-intensive, making it unsuitable for large-scale preparation and application.[14] In this case, nontoxic and environment-friendly biomass directly obtained from nature is a suitable choice for interface modification. Agar is one of the most commonly used polysaccharides in the food industry, which is renowned for its abundant production, nontoxicity, biocompatibility and degradability, particularly for its low price. In addition, its abundant polar functional groups make it possible to improve the electrochemical performance of Zn anodes. Unfortunately, to the best of our knowledge, agar has not been attempted as interface layer to stabilize Zn anodes.

Herein, we develop an interface layer as powerful barrier to inhibit parasitic reactions on anodes of AZIBs by using low-cost and environment-friendly agar via a simple method. The controllable and scalable agar layer prepared without any binder manifests strong adhesion on Zn foil, making it capable to provide durable protection for anodes. The existence of agar layer can enormously restrain the HER and corrosion reaction by blocking the direct contact between Zn metal and electrolyte. Additionally, owing to the electrostatic interaction between polar functional groups on agar and Zn^{2+}, Zn^{2+} migration is greatly accelerated, with the Zn^{2+} transference number increased to 0.60, thus reducing Zn^{2+} concentration gradient and inhibiting Zn dendrite growth. Moreover, this interface layer also plays an important role in suppressing the shuttle of V species from cathodes. As a result, the agar layer

[a] Dr. Y.-F. Qu, Dr. X. Liu, Dr. J.-W. Qian, Prof. L.-F. Chen
CAS Key Laboratory of Mechanical Behavior and Design of Materials (LMBD), School of Engineering Science, School of Chemistry and Materials Science, Division of Nanomaterials & Chemistry, Hefei National Research Center for Physical Sciences at the Microscale, University of Science and Technology of China, Hefei, Anhui 230026, PR China
E-mail: chenlf@ustc.edu.cn

[b] Prof. J. Chen
School of Materials Science and Engineering, Ocean University of China, Qingdao 266100, PR China
E-mail: chenjingwei@ouc.edu.cn

Supporting information for this article is available on the WWW under https://doi.org/10.1002/batt.202400159

Research Article
doi.org/10.1002/batt.202400159
Chemistry Europe
European Chemical Societies Publishing

effectively decreases the kinetics of side reactions and enhances the reversibility of Zn plating/stripping. Zn||A-Cu asymmetric cell shows a high CE of 99.5% for 590 cycles at 5 mA cm^{-2}, and A-Zn symmetric cell manifests an excellent lifespan of 1100 h at 2 mA cm^{-2}, indicating the satisfactory durability and stability of A-Zn anode.

Besides, the capability of practical application is verified by A-Zn||NVO full cell, which can steadily work for 3600 cycles at 5 A g^{-1} with a capacity retention of 94.8%, and the assembled pouch cell can light up LEDs successfully.

Results and Discussion

As shown in Figure 1a, an agar-derived interface layer is constructed on commercial Zn foil by a simple coating method, which mainly involves heating and drying procedures. Besides, toxic reagents as well as advanced equipment are excluded in the preparation process, making it a low-cost and environment-friendly strategy for interface modification on Zn anodes. Compared with most of ex-situ interface layers reported previously, which are easily to peel off due to the weak adhesion on Zn foil,[15] this agar layer shows stronger attachment to Zn anode at different states, guaranteeing its stable and durable protection for Zn anode in the long-term operation (Figure S1). Furthermore, the simple method makes it feasible to extend to large-scale preparation and application, which is preliminarily validated in the laboratory (Figure S2). FTIR is used to analyze the functional groups in agar layer (Figure 1b). The broad absorption peak from 3000 to 3600 cm^{-1} belongs to O–H of agar molecules, and the two peaks at 1038 and 2960 cm^{-1} are indexed to the stretching vibration of C–O and C–H, respectively. These oxygen-contained groups with negative charges are favorable to uniform Zn deposition and inhibition of parasitic reactions, which will be discussed later. Unfortunately, the manufacture and pre-treatment cause the formation of massive scratches on bare Zn foil (Figure 1c), which is detrimental to homogeneous distribution of electrical field and

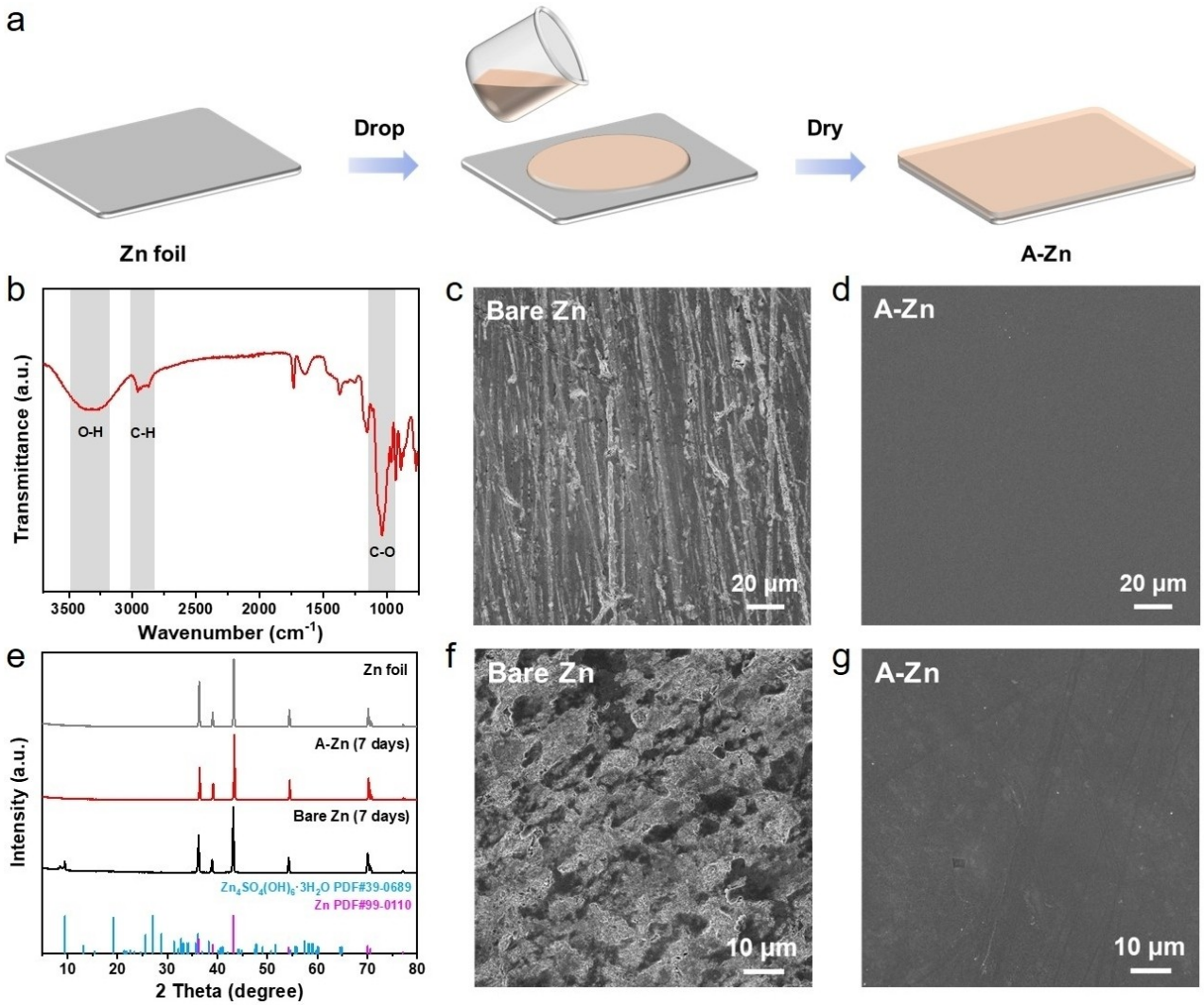

Figure 1. a) Schematic illustration of the preparation of A-Zn. b) FTIR spectrum of the agar layer. SEM images of c) bare Zn and d) A-Zn electrodes. e) XRD patterns of bare Zn and A-Zn electrodes soaked in 2 M $ZnSO_4$ electrolyte for 7 days. SEM images of f) bare Zn and g) A-Zn electrodes after soak.

Zn^{2+}, exacerbating dendrite growth during Zn plating. In comparison, it is obvious that A-Zn electrode exhibits a much smoother surface without any bulges (Figure 1d), which is beneficial to uniform Zn deposition. In order to verify the anti-corrosion role of the interface layer, both bare Zn and A-Zn are soaked in 2 M $ZnSO_4$ electrolyte for a week, and their morphology and chemical composition are investigated subsequently. XRD patterns of the soaked bare Zn and A-Zn electrodes are shown in Figure 1e, and a marked difference can be noticed. Small diffraction peaks around 9° are detected on soaked bare Zn, which are attributed to $Zn_4SO_4(OH)_6 \cdot 3H_2O$ (ZSH) by-products on the surface, verifying the occurrence of corrosion between Zn metal and mildly acidic electrolyte. In comparison, the existence of agar layer can effectively avoid the direct contact between electrolyte and Zn metal, thus enhancing the corrosion-resistance of A-Zn. As a result, XRD pattern of soaked A-Zn remains consistent with that of Zn foil. As illustrated in Figure 1f, the morphology of soaked bare Zn is recorded by SEM. The surface of bare Zn is entirely covered by ZSH nanoflakes, which can passivate anodes and prevent fresh Zn metal from participating in electrochemical reactions. For A-Zn, by-products are negligible with a well-preserved flat surface (Figure 1g). Based on these experimental results, the corrosion-resistance of Zn anode has been improved immensely thanks to the agar interface layer that inhibits parasitic reactions. Before conducting a series of electrochemical tests, the impact of coating thickness on Zn anode performance is discussed by assembling symmetric cells. As shown in Figure S3a, in spite of its lower voltage polarization, the thinner agar layer is inadequate to provide durable protection for long-term operation of A-Zn-50 because of its inferior strength. For A-Zn-200 and A-Zn-400, thicker coating layers are detrimental to Zn^{2+} diffusion, which results in higher voltage polarization and induces dendrite growth, causing the premature failure of symmetric cells (Figure S3c and S3d). In contrast, A-Zn-100 manifests the longest lifespan of 1100 h and moderate voltage polarization (Figure S3b), thus it is selected as the optimum sample to investigate this interface modification strategy. A-Zn-100 is abbreviated to A-Zn and the measured thickness of its agar layer is about 10 μm.

Apart from chemical corrosion, HER is another predominant and spontaneous parasitic reaction in AZIBs. LSV tests are conducted to estimate the HER intensity of the two kinds of electrodes and demonstrate the ability of agar layer to suppress HER. As shown in Figure 2a, with the potential reaching −1.8 V (vs. AgCl/Ag), the HER current of A-Zn is merely $-9.4\ mA\,cm^{-2}$, while the current of bare Zn is up to $-22.5\ mA\,cm^{-2}$, significantly reflecting strong inhibition effect of agar layer on HER. Additionally, the differences between the two electrodes in electrochemical corrosion are presented by linear polarization curves (Figure 2b). Compared with bare Zn, A-Zn electrode manifests more positive corrosion potential and decreased corrosion current, suggesting the tremendously diminished electrochemical corrosion.[16] Considering the above results, the introduced agar interface layer provides shielding effect on HER and corrosion, which reduces the inclination toward parasitic reactions. Furthermore, CA curves are obtained by exerting an overpotential of −150 mV on symmetric cells to investigate the nucleation patterns of Zn^{2+} on bare Zn and A-Zn electrodes (Figure 2c). Obviously, the current is gradually increasing for bare Zn during testing, which represents typical 2D diffusion pattern. In this case, Zn^{2+} tend to diffuse to the most favorable nucleation sites to complete Zn deposition. As a consequence, this heterogeneous deposition gradually turns into uncontrollable dendrite during the following cycling.[17] In contrast, the current of A-Zn maintains constant after a short-time increase, which means that 2D diffusion is successfully converted into 3D diffusion with the help of agar layer. For A-Zn, the close interaction between Zn^{2+} and oxygen-contained groups on agar layer facilitates uniform Zn^{2+} distribution and deposition, suppressing the dramatic dendrite growth. In order to present insight into Zn plating behavior, nucleation overpotential (NOP) of Zn^{2+} is measured by assembling asymmetric cells. As shown in Figure 2d, A-Cu substrate, coated with agar layer, manifests a higher NOP of 36.4 mV than bare Cu (30.1 mV), demonstrating that smaller Zn nuclei are formed on A-Cu electrode according to the nucleation radius formula.[18] Combining CA and NOP tests, it can be deduced that the agar layer is able to promote homogenous and dense Zn deposition, which is favorable to improving the reversibility of Zn plating/stripping.

Coulombic efficiency (CE) of asymmetric cells is an important index to evaluate the reversibility of Zn plating/stripping. The assembled Zn||A-Cu cell can work normally for 400 cycles and achieve a high average CE of 99.5% at the current of $2\ mA\,cm^{-2}$ with a capacity of $1\ mAh\,cm^{-2}$ (Figure 2e). However, CE fluctuation occurs for Zn||bare Cu cell within 80 cycles. After increasing the current density to $5\ mA\,cm^{-2}$, Zn||A-Cu cell shows an excellent lifespan of 590 cycles, and the high CE of 99.5% is also preserved (Figure 2f). In contrast, the CE of Zn||bare Cu drops to 0 at the 192nd cycle abruptly, and the cell breaks down thereafter. Meanwhile, the voltage profiles of Zn||bare Cu at specific cycles are extracted to reveal the cause of cell corrupt. As displayed in Figure 2g, the voltage decreases to 0 V approximately in the discharge profile at the 192nd cycle, suggesting internal short circuit due to the Zn dendrite growth. Therefore, the corresponding charge profile is almost a straight line at 0 V and the cutoff voltage cannot be reached any more. For Zn||A-Cu cell, the chosen charge/discharge profiles overlap well (Figure 2h), indicating that highly reversible Zn plating/stripping is achieved by this interface layer.

The shielding effects of the introduced agar layer on parasitic reactions have been confirmed by the above experimental results, and it is necessary to elucidate the mechanisms in this protective strategy. For bare Zn without any protective measures (Figure 3a), aqueous electrolyte comes into contact with Zn foil directly, so H_2O and SO_4^{2-} are able to access to the surface of Zn foil. Under cathodic current, HER competes with Zn^{2+} reduction reaction and produces abundant H_2 gas, further resulting in an increase of local pH around Zn anodes. Thereafter, Zn^{2+} can react with SO_4^{2-} and OH^- from decomposed H_2O to form ZSH by-products, passivating the fresh Zn metal and impeding further reactions. Meanwhile, chemical corrosion between Zn metal and protons is always taking place as well. Influenced by the parasitic reactions, Zn^{2+} diffuse to the zones

Research Article
doi.org/10.1002/batt.202400159
Chemistry Europe
European Chemical Societies Publishing

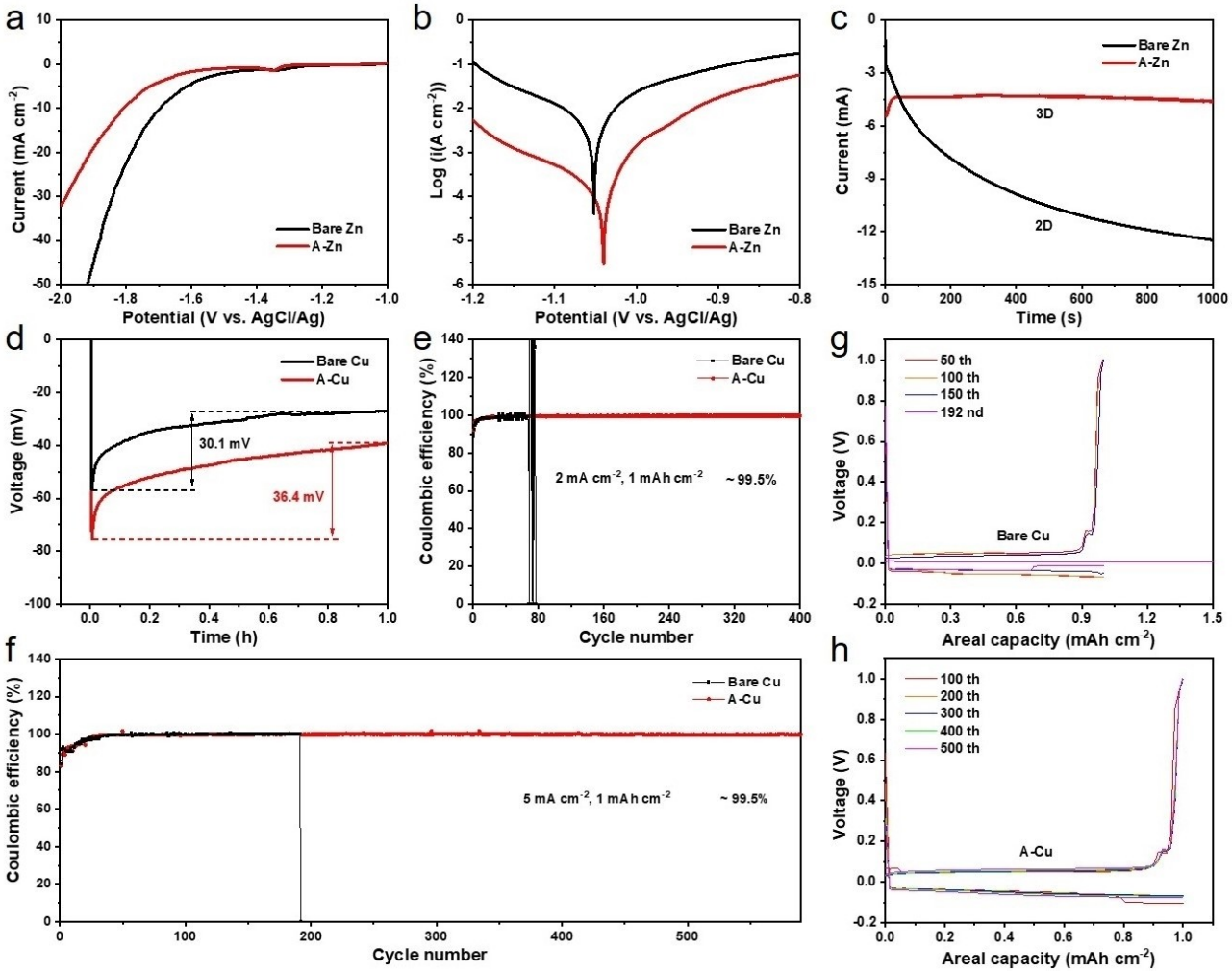

Figure 2. a) LSV curves and b) Tafel plots of bare Zn and A-Zn electrodes. c) CA curves of bare Zn and A-Zn symmetric cells at the overpotential of −150 mV. d) Nucleation overpotential of Zn plating on bare Cu and A-Cu electrodes. Coulombic efficiency of bare Cu and A-Cu asymmetric cells with an areal capacity of 1 mAh cm^{-2} at the current density of e) 2 mA cm^{-2} and f) 5 mA cm^{-2}. Voltage profiles of g) bare Cu and h) A-Cu asymmetric cells with the stripping cutoff voltage of 1.0 V (vs. Zn^{2+}/Zn).

with enriched electrons rather than the passivated areas when plating, hence the Zn dendrite grows uncontrollably. For A-Zn (Figure 3b), thanks to the existence of the agar layer characterized by negatively charged oxygen-contained groups (e.g. hydroxyl and ether groups), SO_4^{2-} are leached out because of strong electrostatic repulsion. The positively charged Zn^{2+}, on the contrary, can pass through the interface layer successfully with the assistance of electrostatic attraction, during which the desolvation process is accelerated and H_2O are left out. Therefore, the origins of side reactions are constricted and Zn^{2+} are evenly distributed, achieving uniform deposition in the end.

Higher reversibility of Zn plating/stripping is conducive to improving durability of Zn anodes in long-term operation. As shown in Figure 3c, A-Zn symmetric cell exhibits an exceptional lifespan of 1100 h at the current of 2 mA cm^{-2} with a capacity of 1 mAh cm^{-2}, exceeding that of bare Zn cell. The voltage reduction after 40 h for bare Zn cell is ascribed to short circuit brought by dendrite growth. Moreover, in the rate performance test (Figure 3d), there is also a short circuit phenomenon for bare Zn symmetric cell when gradually increasing the current density to 5 mA cm^{-2}, suggesting bare Zn anodes cannot adapt to variation in operating conditions. Instead, A-Zn cell is able to stably work for a long time no matter how the current changes. EIS curves are used to analyze interfacial resistance of the two kinds of Zn anodes (Figure 3e and S4). It can be seen that A-Zn manifests a smaller charge transfer resistance than bare Zn, which means that the desolvation process is accelerated by the interaction between Zn^{2+} and agar layer. In addition, the Zn^{2+} transfer is boosted by electrostatic attraction between Zn^{2+} and agar molecules. For instance, the measured Zn^{2+} transference number (t_{Zn}^{2+}) of A-Zn cell is as high as 0.60 (Figure 3f). The higher t_{Zn}^{2+} means that Zn^{2+} are dominant charge carriers, and the Zn^{2+} concentration gradient on electrodes is diminished as well.[19] Correspondingly, the transport of SO_4^{2-} is severely hampered because of electrostatic repulsion between SO_4^{2-} and negatively charged groups on agar layer, thus reducing the probability of by-product formation. However, the t_{Zn}^{2+} of bare

Research Article
doi.org/10.1002/batt.202400159
Chemistry Europe
European Chemical Societies Publishing

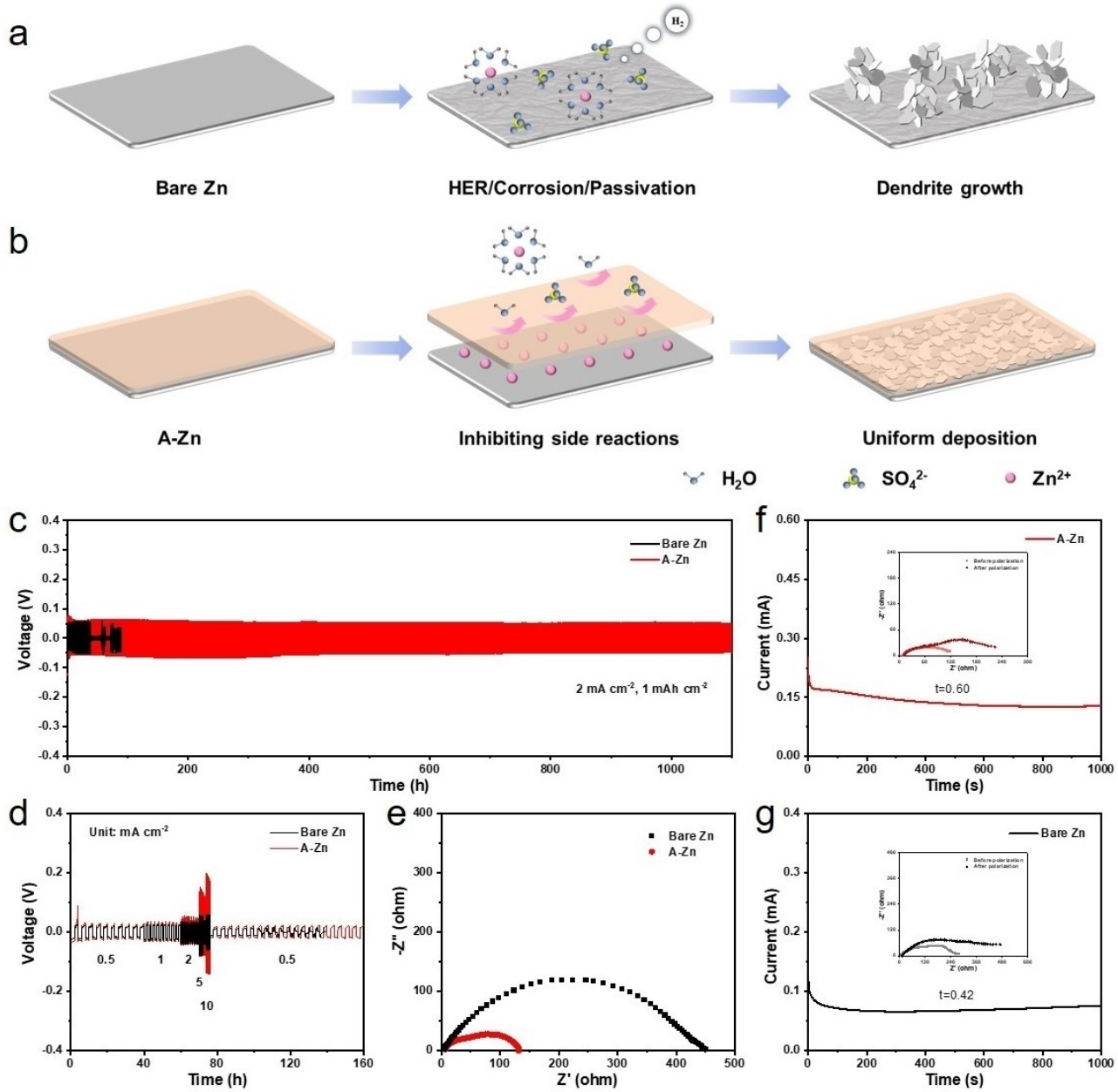

Figure 3. Schematic illustration of different Zn deposition patterns on a) bare Zn and b) A-Zn. c) Cycling performance of bare Zn and A-Zn symmetric cells with an areal capacity of 1 mAh cm^{-2} at the current density of 2 mA cm^{-2}. d) Rate performance of symmetric cells with a constant areal capacity of 1 mAh cm^{-2}. e) EIS curves of bare Zn and A-Zn symmetric cells. Zn^{2+} transference number of f) A-Zn and g) bare Zn symmetric cells.

Zn cell is merely 0.42 (Figure 3g), which has little influence on inhibition of Zn dendrite and parasitic reactions.

After testing cycling performance of symmetric cells, the cycled electrodes are subjected to post-mortem characterizations. The surface morphology of cycled bare Zn and A-Zn is recorded in SEM images (Figure 4a). After the initial 5 cycles, huge bulge-like deposits begin to emerge on bare Zn, representing the origin of Zn dendrite. As expected, typical dendrite structure embedded with glass fibers appears in the later cycles, which can pierce through the separator and result in short circuit during long-term cycling. In contrast, A-Zn shows relatively homogeneous and dense Zn deposition without dendrite, further verifying the positive effect of agar layer on regulating Zn plating behavior. Besides, little peaks attributed to ZSH by-products can be identified in the XRD pattern of cycled bare Zn electrode, while these peaks are absent for cycled A-Zn (Figure 4b), demonstrating the powerful capability of agar layer to alleviate parasitic reactions. With less by-product accumulation on the surface of electrodes, the cycled A-Zn symmetric cell exhibits smaller charge transfer resistance than bare Zn cell (Figure 4c, 4d and S5).

The full cells of AZIBs using NVO cathodes are assembled to estimate the practical application potential of this interface modified Zn anode. As shown in Figure 5a, bare Zn||NVO and

Research Article
doi.org/10.1002/batt.202400159
Chemistry Europe
European Chemical Societies Publishing

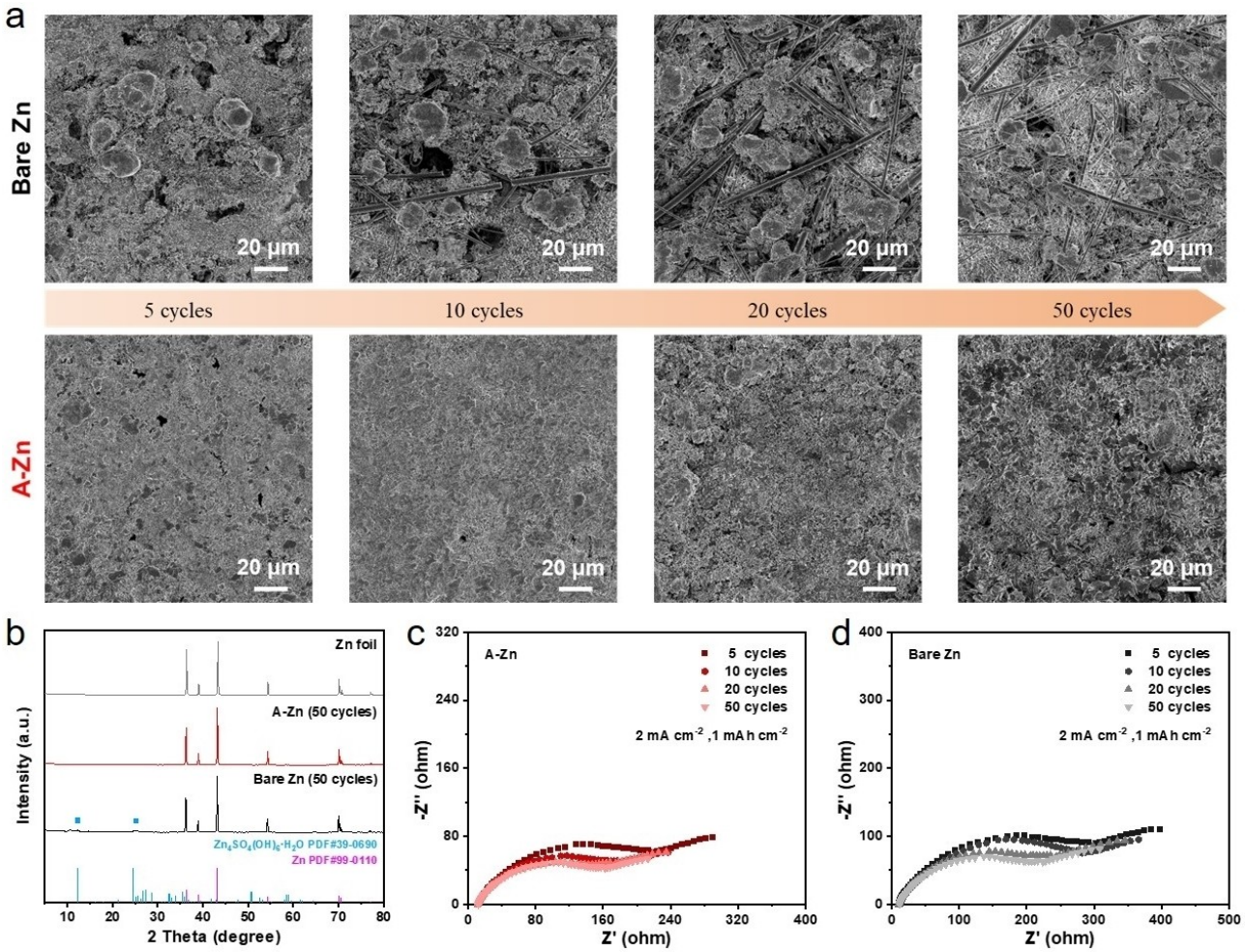

Figure 4. a) SEM images of bare Zn and A-Zn electrodes after various cycles at 2 mA cm^{-2} with a capacity of 1 mAh cm^{-2}. b) XRD patterns of bare Zn and A-Zn electrodes in symmetric cells after 50 cycles. EIS curves of c) A-Zn and d) bare Zn symmetric cells after 5, 10, 20 and 50 cycles.

A-Zn||NVO cells exhibit almost identical CV curves, indicating the redox reaction remains unchanged after introducing agar layer. According to the EIS curves (Figure 5b and S6), both charge transfer resistance and ion diffusion resistance of A-Zn||NVO cell are smaller than those of bare Zn||NVO cell, reflecting the promoted desolvation process and transport of Zn^{2+} provided by agar layer. Consequently, the capacity of A-Zn||NVO is 389.8, 335.9, 293.6, 248.5 and 186.1 mAh g^{-1} at the current density of 0.2, 0.5, 1.0, 2.0 and 5.0 A g^{-1}, respectively, indicating better rate performance than bare Zn||NVO (Figure 5c). In the long-term cycling test of full cells (Figure 5d), A-Zn||NVO can steadily operate for 3600 cycles at 5 A g^{-1} with an outstanding capacity retention of 94.8%, while noticeable CE fluctuation and capacity deterioration happen within 1700 cycles for bare Zn||NVO cell. The SEM image of cycled bare Zn anode in full cell unveils the reason for capacity decay (Figure 5e). Dramatic dendrite entangled with glass fibers appears on the surface of bare Zn, meaning that the premature failure results from partial short circuit. In comparison, more uniform Zn deposition can be observed on cycled A-Zn anode (Figure 5f), which is favorable to obtaining better electrochemical performance. Moreover, the inhibition effect of agar layer on the shuttle of V species is verified by H-type glass cells, demonstrating that the interface layer can prevent V species from damaging anodes simultaneously (Figure S7). Afterward, A-Zn||NVO pouch cells are assembled to assess the feasibility for large-scale development. As illustrated in the inset of Figure 5g, two pouch cells in series can light up red LEDs successfully. Moreover, the pouch cell presents a long lifespan of 300 cycles with 220.9 mAh g^{-1} remained at 1 A g^{-1}.

Conclusions

In summary, based on low-cost and environment-friendly agar, an effective interface modification strategy for Zn anodes of AZIBs is proposed to suppress parasitic reactions and dendrite growth. This agar layer can work as a powerful barrier between electrolyte and Zn metal, hence greatly reducing HER and corrosion on anodes. The abundant functional groups on agar can induce uniform Zn^{2+} distribution and deposition through electrostatic interaction. As a result, Zn||A-Cu asymmetric cell owns a high average CE of 99.5% for 590 cycles, and A-Zn symmetric cell can operate for 1100 h at 2 mA cm^{-2}, suggesting

Research Article
doi.org/10.1002/batt.202400159
Chemistry Europe
European Chemical Societies Publishing

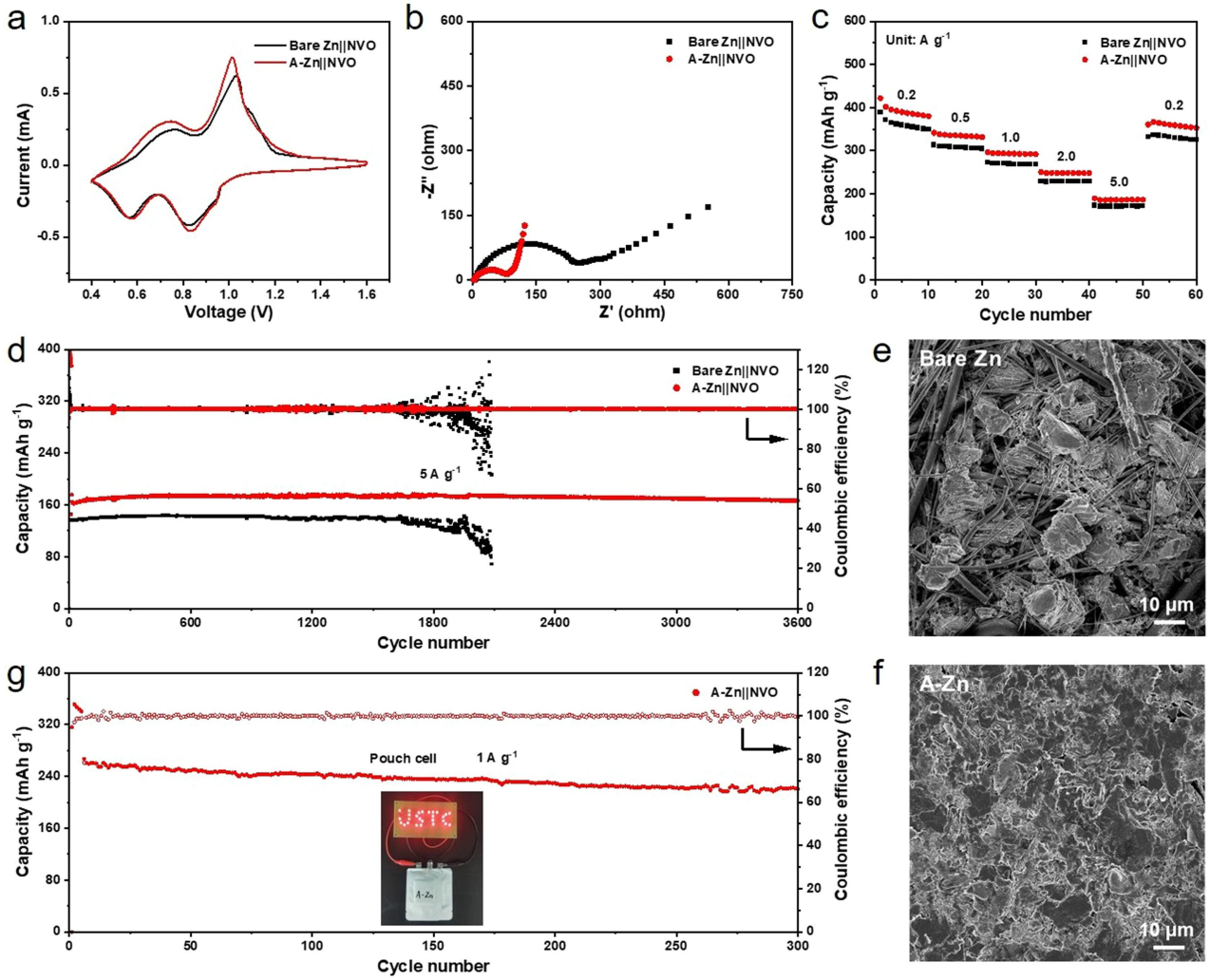

Figure 5. a) CV curves of bare Zn||NVO and A-Zn||NVO full cells at the scan rate of 0.1 mV s^{-1}. b) Nyquist plots of bare Zn||NVO and A-Zn||NVO full cells. c) Rate performance of bare Zn||NVO and A-Zn||NVO full cells. d) Cycling performance of bare Zn||NVO and A-Zn||NVO full cells at the current density of 5 A g^{-1}. SEM images of e) bare Zn and f) A-Zn anodes in full cells after 100 cycles. g) Cycling performance of A-Zn||NVO pouch cell at the current density of 1 A g^{-1} with the inset showing the digital photograph of pouch cell lighting up LEDs.

outstanding reversibility of Zn plating/stripping and durability of A-Zn anode. Notably, the stable A-Zn anode offers 94.8% capacity retention after 3600 cycles at 5 A g^{-1} for A-Zn||NVO full cell, showing great potential of practical application. Therefore, this work offers a facile and effective strategy for developing ultra-stable and high-performance AZIBs.

Experimental Section

Preparation of A-Zn and A-Cu electrodes: For A-Zn, 0.1 g agar powder was dissolved in 9.9 g deionized water at 90 °C by mechanical stirring, forming a translucent slurry. The slurry was coated on clean Zn foil (80 μm) using doctor blades (50, 100, 200, and 400 μm) and dried at 40 °C in a vacuum oven. A-Cu electrode was prepared in a similar way, only by replacing Zn foil with Cu foil.

Preparation of sodium vanadate (NVO) cathodes: The synthesis method of NVO material can be found in a previous literature.[20] Typically, 2 g V_2O_5 powder was added into 30 mL NaCl aqueous solution (2 M), and the mixture was stirred at 30 °C for 96 h. Then the NVO material was obtained after washing and freeze-drying. To fabricate the cathodes, NVO, carbon black and polyvinylidene fluoride (PVDF) was dissolved in N-methyl-2-pyrrolidone (NMP) at the mass ratio of 7:2:1 to form black slurry which was coated on stainless steel mesh subsequently. Afterward, NVO cathodes were obtained after drying the mesh with slurry at 80 °C in a vacuum oven, and the mass loading of NVO is 2.0 ± 0.5 mg cm^{-2}.

Material Characterizations: Thermo Scientific Nicolet 8700 was used to collect Fourier transform infrared (FTIR) absorption spectra. X-ray diffraction (XRD) tests were conducted on ARL EQUINOX 3000 using a Cu Kα radiation source. Scanning electron microscopy (SEM) and Energy-dispersive X-ray spectroscopy (EDX) analyses were obtained on ZEISS GeminiSEM 450.

Electrochemical measurements: Linear sweep voltammetry (LSV), Chronoamperometry (CA), Cyclic voltammetry (CV), Electrochemical impedance spectroscopy (EIS) and Tafel plots were tested on electrochemical workstation (Shanghai Chenhua, CHI-760E). Three-electrode system was used for LSV and Tafel tests, where Pt and Ag/AgCl were used as counter electrode and reference electrode, respectively. Charge/discharge tests of cells were conducted on LAND CT3001A in the form of coin cells (CR2032). Specifically,

symmetric cells consisted of two bare Zn (or A-Zn) electrodes, and asymmetric cells were assembled by using bare Zn and bare Cu (or A-Cu) as anodes and cathodes, respectively. The electrolyte and separator were 2 M $ZnSO_4$ aqueous solution and glass fibers (GF/D), respectively. The full cells used bare Zn (or A-Zn) and NVO as anodes and cathodes, respectively, and 1 M Na_2SO_4 was added into 2 M $ZnSO_4$ to inhibit the dissolution of cathode material. The diameter of electrodes in coin cells is 10 mm, while the size of electrodes in pouch cells is 3 cm×4 cm.

Acknowledgements

This work was financially supported by the National Natural Science Foundation of China (U2230101), Anhui Provincial Hundred Talents Program, Anhui Provincial Major Science and Technology Project (202203a05020048), USTC Startup Program (KY2090000062, KY2090000098, KY2090000099), and Joint Research Center for Multi-Energy Complementation and Conversion. The data was partially obtained at the USTC Center for Micro and Nanoscale Research and Fabrication.

Conflict of Interests

The authors declare no conflict of interest.

Data Availability Statement

The data that support the findings of this study are available from the corresponding author upon reasonable request.

Keywords: aqueous zinc-ion batteries · Zn anode · interface layer · agar · parasitic reactions

[1] a) J. Ran, M. Jaroniec, S.-Z. Qiao, *Adv. Mater.* **2018**, *30*, 1704649; b) E. Kabir, P. Kumar, S. Kumar, A. A. Adelodun, K.-H. Kim, *Renewable Sustainable Energy Rev.* **2018**, *82*, 894–900.
[2] a) F. Wu, J. Maier, Y. Yu, *Chem. Soc. Rev.* **2020**, *49*, 1569–1614; b) J.-Y. Hwang, S.-T. Myung, Y.-K. Sun, *Chem. Soc. Rev.* **2017**, *46*, 3529–3614; c) W. Zhang, Y. Liu, Z. Guo, *Sci. Adv.* **2019**, *5*, eaav7412.
[3] a) F. Ming, Y. Zhu, G. Huang, A.-H. Emwas, H. Liang, Y. Cui, H. N. Alshareef, *J. Am. Chem. Soc.* **2022**, *144*, 7160–7170; b) P. Ruan, S. Liang, B. Lu, H. J. Fan, J. Zhou, *Angew. Chem. Int. Ed.* **2022**, *61*, e202200598; c) J.-J. Ye, P.-H. Li, H.-R. Zhang, Z.-Y. Song, T. Fan, W. Zhang, J. Tian, T. Huang, Y. Qian, Z. Hou, N. Shpigel, L.-F. Chen, S. X. Dou, *Adv. Funct. Mater.* **2023**, *33*, 2305659.
[4] a) G. Ma, L. Miao, Y. Dong, W. Yuan, X. Nie, S. Di, Y. Wang, L. Wang, N. Zhang, *Energy Storage Mater.* **2022**, *47*, 203–210; b) J.-L. Yang, J. Li, J.-W. Zhao, K. Liu, P. Yang, H. J. Fan, *Adv. Mater.* **2022**, *34*, 2202382; c) J.-H. Wang, W.-X. Dong, J. Chen, L.-F. Chen, *Ionics* **2023**, *29*, 3097–3107.
[5] a) F. Wang, O. Borodin, T. Gao, X. Fan, W. Sun, F. Han, A. Faraone, J. A. Dura, K. Xu, C. Wang, *Nat. Mater.* **2018**, *17*, 543–549; b) T. C. Li, Y. Lim, X. L. Li, S. Luo, C. Lin, D. Fang, S. Xia, Y. Wang, H. Y. Yang, *Adv. Energy Mater.* **2022**, *12*, 2103231; c) Z. Shen, J. Mao, G. Yu, W. Zhang, S. Mao, W. Zhong, H. Cheng, J. Guo, J. Zhang, Y. Lu, *Angew. Chem. Int. Ed.* **2023**, *62*, e202218452; d) Y. Li, P. Wu, W. Zhong, C. Xie, Y. Xie, Q. Zhang, D. Sun, Y. Tang, H. Wang, *Energy Environ. Sci.* **2021**, *14*, 5563–5571.
[6] a) J.-H. Wang, L.-F. Chen, W.-X. Dong, K. Zhang, Y.-F. Qu, J.-W. Qian, S.-H. Yu, *ACS Nano* **2023**, *17*, 19087–19097; b) H. He, L. Zeng, D. Luo, J. He, X. Li, Z. Guo, C. Zhang, *Adv. Mater.* **2023**, *35*, 2211498; c) Y. Zeng, X. Zhang, R. Qin, X. Liu, P. Fang, D. Zheng, Y. Tong, X. Lu, *Adv. Mater.* **2019**, *31*, 1903675; d) C. Xie, H. Ji, Q. Zhang, Z. Yang, C. Hu, X. Ji, Y. Tang, H. Wang, *Adv. Energy Mater.* **2023**, *13*, 2203203.
[7] a) L. Yao, C. Hou, M. Liu, H. Chen, Q. Zhao, Y. Zhao, Y. Wang, L. Liu, Z.-W. Yin, J. Qiu, S. Li, R. Qin, F. Pan, *Adv. Funct. Mater.* **2022**, *33*, 2209301; b) L. Yao, G. Wang, F. Zhang, X. Chi, Y. Liu, *Energy Environ. Sci.* **2023**, *16*, 4432–4441; c) Z. Zheng, S. Guo, M. Yan, Y. Luo, F. Cao, *Adv. Mater.* **2023**, *35*, 2304667; d) Y. Fang, X. Xie, B. Zhang, Y. Chai, B. Lu, M. Liu, J. Zhou, S. Liang, *Adv. Funct. Mater.* **2022**, *32*, 2109671.
[8] a) M. Fu, H. Yu, S. Huang, Q. Li, B. Qu, L. Zhou, G.-C. Kuang, Y. Chen, L. Chen, *Nano Lett.* **2023**, *23*, 3573–3581; b) J. Zhou, Y. Mei, F. Wu, Y. Hao, W. Ma, L. Li, M. Xie, R. Chen, *Angew. Chem. Int. Ed.* **2023**, *62*, e202304454; c) S. Zhai, W. Song, K. Jiang, X. Tan, W. Zhang, Y. Yang, W. Chen, N. Chen, H. Zeng, H. Li, Z. Li, *Energy Environ. Sci.* **2023**, *16*, 5479–5489; d) F. Zhang, J. Qian, W. Dong, Y. Qu, J. Chen, H. Wang, L.-F. Chen, *Chem. Eng. J.* **2023**, *478*, 147406; e) W. Li, Q. Zhang, Z. Yang, H. Ji, T. Wu, H. Wang, Z. Cai, C. Xie, Y. Li, H. Wang, *Small* **2022**, *18*, 2205667.
[9] C. Nie, G. Wang, D. Wang, M. Wang, X. Gao, Z. Bai, N. Wang, J. Yang, Z. Xing, S. Dou, *Adv. Energy Mater.* **2023**, *13*, 2300606.
[10] a) J. Hao, B. Li, X. Li, X. Zeng, S. Zhang, F. Yang, S. Liu, D. Li, C. Wu, Z. Guo, *Adv. Mater.* **2020**, *32*, e2003021; b) P. Xiao, Y. Wu, K. Liu, X. Feng, J. Liang, Y. Zhao, C. Wang, X. Xu, T. Zhai, H. Li, *Angew. Chem. Int. Ed.* **2023**, *62*, e202309765; c) X. Zhou, P. Cao, A. Wei, A. Zou, H. Ye, W. Liu, J. Tang, J. Yang, *ACS Appl. Mater. Interfaces* **2021**, *13*, 8181–8190; d) Q. Zou, Z. Liang, W. Wang, D. Dong, Y.-C. Lu, *Energy Environ. Sci.* **2023**, *16*, 6026–6034.
[11] a) Y. Zhou, J. Xia, J. Di, Z. Sun, L. Zhao, L. Li, Y. Wu, L. Dong, X. Wang, Q. Li, *Adv. Energy Mater.* **2023**, *13*, 2203165; b) X. Luan, L. Qi, Z. Zheng, Y. Gao, Y. Xue, Y. Li, *Angew. Chem. Int. Ed.* **2023**, *62*, e202215968.
[12] a) J. Zheng, X. Liu, Y. Zheng, A. N. Gandi, X. Kuai, Z. Wang, Y. Zhu, Z. Zhuang, H. Liang, *Nano Lett.* **2023**, *23*, 6156–6163; b) W. Liu, Q. Zhao, H. Yu, H. Wang, S. Huang, L. Zhou, W. Wei, Q. Zhang, X. Ji, Y. Chen, L. Chen, *Adv. Funct. Mater.* **2023**, *33*, 2302661; c) T. Wang, Y. Tang, M. Yu, B. Lu, X. Zhang, J. Zhou, *Adv. Funct. Mater.* **2023**, *33*, 2306101.
[13] a) B. Li, S. Liu, Y. Geng, C. Mao, L. Dai, L. Wang, S. C. Jun, B. Lu, Z. He, J. Zhou, *Adv. Funct. Mater.* **2023**, *34*, 2214033; b) X. Zeng, K. Xie, S. Liu, S. Zhang, J. Hao, J. Liu, W. K. Pang, J. Liu, P. Rao, Q. Wang, J. Mao, Z. Guo, *Energy Environ. Sci.* **2021**, *14*, 5947–5957; c) Z. Zhao, J. Zhao, Z. Hu, J. Li, J. Li, Y. Zhang, C. Wang, G. Cui, *Energy Environ. Sci.* **2019**, *12*, 1938–1949.
[14] a) X. Chen, W. Li, D. Reed, X. Li, X. Liu, *Electrochem. Energy Rev.* **2023**, *6*, 33; b) F. Tao, Y. Liu, X. Ren, J. Wang, Y. Zhou, Y. Miao, F. Ren, S. Wei, J. Ma, *J. Energy Chem.* **2022**, *66*, 397–412; c) C. Deng, X. Xie, J. Han, B. Lu, S. Liang, J. Zhou, *Adv. Funct. Mater.* **2021**, *31*, 2103227.
[15] H. He, H. Qin, J. Wu, X. Chen, R. Huang, F. Shen, Z. Wu, G. Chen, S. Yin, J. Liu, *Energy Storage Mater.* **2021**, *43*, 317–336.
[16] J. Li, S. Zhou, Y. Chen, X. Meng, A. Azizi, Q. He, H. Li, L. Chen, C. Han, A. Pan, *Adv. Funct. Mater.* **2023**, *33*, 2307201.
[17] Q. Zong, B. Lv, C. Liu, Y. Yu, Q. Kang, D. Li, Z. Zhu, D. Tao, J. Zhang, J. Wang, Q. Zhang, G. Cao, *ACS Energy Lett.* **2023**, *8*, 2886–2896.
[18] H. Cao, X. Zhang, B. Xie, X. Huang, F. Xie, Y. Huo, Q. Zheng, R. Zhao, Q. Hu, L. Kang, S. Liu, D. Lin, *Adv. Funct. Mater.* **2023**, *33*, 2305683.
[19] X. Cai, W. Tian, Z. Zhang, Y. Sun, L. Yang, H. Mu, C. Lian, H. Qiu, *Adv. Mater.* **2023**, *36*, 2307727.
[20] F. Wan, L. Zhang, X. Dai, X. Wang, Z. Niu, J. Chen, *Nat. Commun.* **2018**, *9*, 1656.

Manuscript received: March 6, 2024
Revised manuscript received: April 4, 2024
Accepted manuscript online: April 16, 2024
Version of record online: May 13, 2024